ARTICLE Communicated by Alain Destexhe

Synchronized Action of Synaptically Coupled Chaotic Model Neurons

Henry D. I. Abarbanel
Department of Physics and Marine Physical Laboratory, Scripps Institution of Oceanography, University of California–San Diego, La Jolla, CA 92093-0402 USA
Institute for Nonlinear Science, University of California–San Diego, La Jolla, CA 92093-0402 USA

R. Huerta
Institute for Nonlinear Science, University of California–San Diego, La Jolla, CA 92093-0402 USA

M. I. Rabinovich
Institute for Nonlinear Science, University of California–San Diego, La Jolla, CA 92093-0402 USA

N. F. Rulkov
Institute for Nonlinear Science, University of California–San Diego, La Jolla, CA 92093-0402 USA

P. F. Rowat
Department of Biology, University of California–San Diego, La Jolla, CA 92093-0357 USA

A. I. Selverston
Department of Biology, University of California–San Diego, La Jolla, CA 92093-0357 USA

Experimental observations of the intracellular recorded electrical activity in individual neurons show that the temporal behavior is often chaotic. We discuss both our own observations on a cell from the stomatogastric central pattern generator of lobster and earlier observations in other cells.

In this paper we work with models of chaotic neurons, building on models by Hindmarsh and Rose for bursting, spiking activity in neurons. The key feature of these simplified models of neurons is the presence of coupled slow and fast subsystems. We analyze the model neurons using the same tools employed in the analysis of our experimental data.

Neural Computation **8, 1567–1602** (1996)

We couple two model neurons both electrotonically and electrochemically in inhibitory and excitatory fashions. In each of these cases, we demonstrate that the model neurons can synchronize in phase and out of phase depending on the strength of the coupling. For normal synaptic coupling, we have a time delay between the action of one neuron and the response of the other. We also analyze how the synchronization depends on this delay. A rich spectrum of synchronized behaviors is possible for electrically coupled neurons and for inhibitory coupling between neurons. In synchronous neurons one typically sees chaotic motion of the coupled neurons. Excitatory coupling produces essentially periodic voltage trajectories, which are also synchronized. We display and discuss these synchronized behaviors using two "distance" measures of the synchronization.

1 Introduction

Individual neurons coupled synaptically to form small functional networks or central pattern generators (CPG) have cooperative properties related to the function they are called on to perform. The cooperative behavior of these coupled cells can be much richer and much more organized than the activity of the individual neurons forming the CPG. The isolated neural cells often exhibit chaotic motions as observed in the characteristics of intracellular voltage measurements (Hayashi and Ishizuka 1992; Aihara and Matsumoto 1986), while some coordination or synchronization of these chaotic activities must be arranged for the directed cooperative behavior of the CPGs to manifest themselves. Our goal in this paper is to demonstrate, by examining the synaptic coupling of model neurons, the interesting broad range of cooperative behaviors that arise when chaotic neurons are connected. Further, we want to understand how it is possible that the potentially very complex behaviors that might transpire when chaotic neurons are coupled in fact reduce in a clean, dynamic way to rather simpler, often well-organized motion, even for nonsymmetrical coupling and nonidentical neurons.

Starting from the classical Hodgkin-Huxley (Hodgkin and Huxley 1952) formulation of the dynamics of ionic channels, numerous simpler "reduced" models have been derived and extensively discussed (Rinzel and Ermentrout 1989). To capture both the bursting behavior and the spiking behavior observed in intracellular voltage measurements, one requires a combination of slow and fast subsystems acting in coordination. The fast subsystem is associated with the membrane voltage and rapid conduction channels, typically those due to Na^+ and K^+. The slow subsystem is critical for bursting behavior on top of which the spikes occur.

The differences among the many models with fast and slow subsystems are characterized by the details of how individual neurons, ab-

stracted to such simplified descriptions, produce spikes and bursts, but each contains the main qualitative behaviors seen in the laboratory. Here we are primarily concerned with the manner in which these neurons act in a cooperative fashion as a result of their synaptic coupling to each other. In this work we have focused on the rich variety of features that can arise through this coupling. An important goal of our research effort is to determine the dynamic variables of such models that are predictive and have sound physiological grounding. To this end we begin with the analysis of data from an isolated neuron from the lobster stomatogastric CPG, then turn to the analysis of model neurons, and from our analyses subsequently turn to the study of further laboratory experiments.

For this we have adopted as our description for individual neurons the rather simple three-degree-of-freedom model discussed by Rose and Hindmarsh (RH) (Hindmarsh and Rose 1984; Rose and Hindmarsh 1985). This model has as dynamical variables the membrane potential, an auxiliary variable corresponding to the various ionic channels, and a slow variable associated with other ion dynamics. The model shows bursting, spike phenomena and chaotic bursting and spiking. All of these neural actions are seen in measurements on neurons in the laboratory (Hayashi and Ishizuka 1992; Selverston 1996).

In this paper we concentrate on the synchronized behavior of chaotic RH neurons when they are coupled by the various types of chemical and electrical synapses coupling observed in nature. Both excitatory and inhibitory forms of chemical synapses will be considered. There are two main issues in beginning this analysis: (1) the chaotic property of the individual neuron dynamics and (2) the interpretation of synchronized behavior when two such chaotic neurons are coupled.

2 Individual Neurons

Rose and Hindmarsh (Hindmarsh and Rose 1984; Rose and Hindmarsh 1985) study a variety of model neurons that are cast into a few ordinary differential equations describing the membrane potential and various aspects of ion conduction important for various functions. Some of their models are two-dimensional; however, such models can never exhibit the chaotic bursting and spiking seen in real neurons. In this regard, they may be seen as oversimplifications of actual neurons that contain numerous types and numbers of channels and may have tens of dynamic degrees of freedom. RH also study three-degree-of-freedom models that, happily, exhibit the broader range of features, including chaotic bursting, seen in laboratory experiments on isolated neurons (Hayashi and Ishizuka 1992). Even these three-dimensional models, however, ignore many ion channels that would, perhaps, be required to extract detailed behavior of any real neuron.

In preparation for adopting one of the three-dimensional models of RH for our study of coupling between chaotic neurons, we begin with an analysis of some experimental observations on real neurons.

2.1 Observed Low-Dimensional Behavior of Neurons. We will be emphasizing the synchronization among model neurons that individually exhibit chaotic behavior. To give a rationale for this emphasis, we first discuss the observed complex dynamical behavior of an isolated cell from the lobster stomatogastric (STG) CPG as observed in our laboratories, that is, an LP neuron from a pyloric CPG. Neurons were isolated from their physiological connections with other neurons in the STG systems by either placing dissociated neurons in culture or by pharmacological blockage of synaptic connections.

The justification of the chaotic behavior in real time series, in particular neural ones, has the unavoidable difficulty of noise interference. Although we cannot mathematically rigorously prove that the LP neuron possesses chaotic behavior, we intend to provide indications that support that the behavior of LP neuron is related to complex or even chaotic dynamics. In this section we will be able to show that the external or internal source of noise cannot suppress traces of a complex low-dimensional system. To help us in this purpose, we study the dynamics of the LP neuron for different values of a control parameter (the injected current).

The data consist of intracellular voltage taken at a data rate of 2 kHz. The sampling time is $\tau_s = 0.5$ ms. Time series for different values of the current applied to the LP neuron are shown in Figure 1. For each time series we have a total of 10^5 data points available for analysis—around 1 minute of real time data.

2.1.1 Attractors and Noise. The time series depicted in Figure 1a, 1b, and 1c appear periodic with noise that slightly changes the phase of the spikes. It is reasonable to assume that the noise has about the same level for all studied values of applied current, because the conditions of the experiments were the same for these values of the current. That means that Fourier power spectrum can give some important information about changing qualitative properties of the time series for different currents and about the onset of chaos. In Figure 2a we display the Fourier power spectrum of quasi-regular spiking behavior (see Fig. 1a) and the spectrum of the spiking, bursting behavior (see Fig. 1d). The level of the power of irregular pulsation in the second case is 10 times larger than the power level of the noise in the quasi-regular time series with current $I = 2$ nA (see also Fig. 3a). This means that the second case is either chaotic dynamics or nonlinear amplification of noise. The next step is the discussion of the differences between these two different phenomena.

The main feature of dynamical chaos is the existence of instability of the motion. In the system phase space, that means that the trajecto-

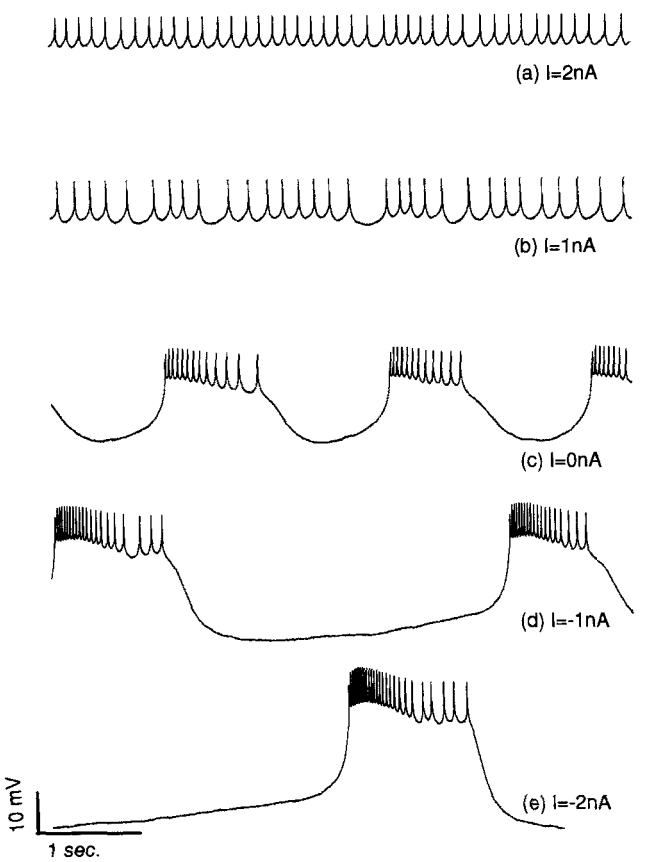

Figure 1: Membrane potentials of the LP neuron for several values of the applied current. (a) $I = 2$ nA. (b) $I = 1$ nA. (c) $I = 0$ nA. (d) $I = -1$ nA. (e) $I = -2$ nA.

ries forming a chaotic attractor are unstable. Except for some particular cases, the action of small amounts of noise does not alter the properties of dynamical chaos in any significant manner. Noise transfers the motion of the system from one trajectory to another, but these trajectories correspond to the same chaotic attractor, which is only slightly changed by noise.

Small noise can qualitatively change the properties of the orbits if the system generating the time series is not structurally stable. To test these possibilities, we reconstruct the phase portraits of the observed motion in some embedding space for different values of a control parameter (ap-

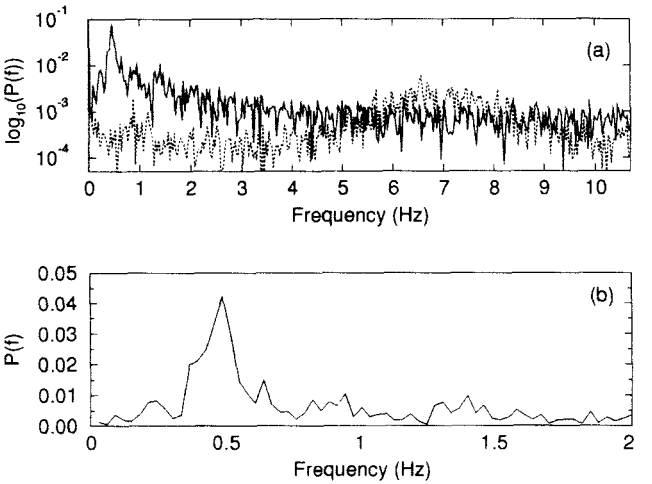

Figure 2: (a) Fourier power spectra for $I = 2$ nA (dotted line) and $I = 0$ nA (solid line). (b) Power spectra for $I = 0$ nA. One may observe the sharp peak corresponding to the bursting oscillations and the broader spectrum for spiking oscillations.

plied current). These results are depicted in Figure 3. Figures 3a and 3b depict limit cycles with some level of noise. Two important messages are extracted from these figures: first, the system is structurally stable because both limit cycles are topologically equivalent for different values of the current; second, the thickness of the attractors, which corresponds to the level of noise, is not changing. Figures 3d and 3c persuade us that we have dynamical chaos here because, despite the presence of noise, the attractors have a very clear robust substructure, which indicates the exponential instability of the trajectories. The spreading of the fast motions on the attractor appears due to the onset of chaos not due to noise. Finally, we observe that in this case, chaos is connected with the fast motion, that is, spiking behavior. The power Fourier spectrum for applied current $I = 0$ nA (see Fig. 2b) shows a strong peak, which corresponds to the periodicity of slow motion. This observation is important when we consider the number of points in the time series required for estimation of embedding dimensions and Lyapunov exponents.

2.1.2 Analysis of Observed Data. To establish which of these alternatives to choose, we must create from the observed voltage measurements $v(n) = v(t_0 + n\tau_s)$ a coordinate system in which the degrees of freedom

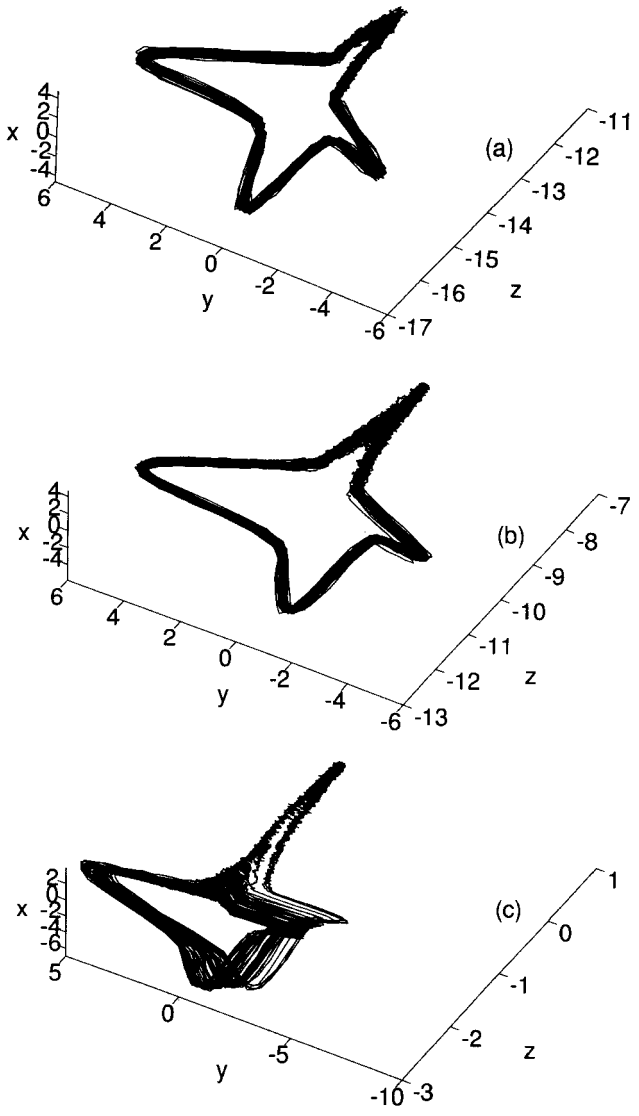

Figure 3: State-space reconstructions from the isolated LP neuron for different values of the current. They have been obtained applying singular value decomposition to a time-delay state space reconstruction using a time delay of 5 msec, which is 10 times the sampling time. This rotates and scales the original coordinates so that the fast spiking motion takes place in the plane x-y and the slow, bursting motion moves along the z-axis. (a) $I = 2$ nA. (b) $I = 1$ nA. (c) $I = 0$ nA.

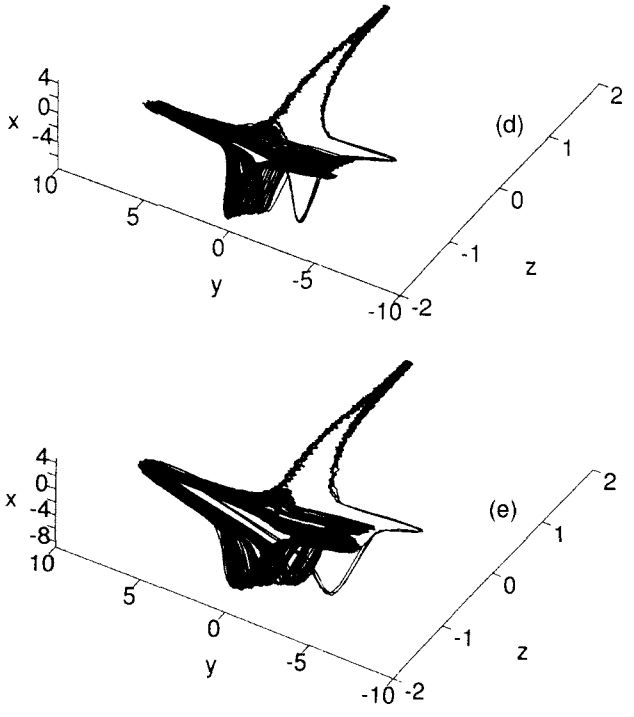

Figure 3: *Continued.* (d) $I = -1$ nA. (e) $I = -2$ nA.

are unfolded from their projection on the observation axis of intracellular voltage. If the system is low-dimensional, a few independent coordinates made from $v(n)$ and its time lags $v(n+kT) = v(t_0 + (n+kT)\tau_s)$ will suffice to unfold the geometric structure typical of a nonlinear dynamical system (Abarbanel *et al.* 1993; Abarbanel 1995). If the observed time sequence is chaotic, this geometric structure, the attractor of the neuronal system, must be embedded in a coordinate system with dimension three or greater. This means we need to construct vectors in some d-dimensional space within which the neuron moves in time. The structure is parametrically labeled by time, which is discrete because of the realities of the measurement process. The vectors

$$\mathbf{y}(n) = [v(n).v(n+T).....v(n+(d-1)T)] \tag{2.1}$$

provide a workable coordinate system in which to unfold the projection of the multidimensional dynamics onto the voltage axis. An initial question that must be answered has to do with the independence of the components of the d-dimensional data vectors $\mathbf{y}(n)$; a nonlinear answer

to this question is contained in the average mutual information (Abarbanel 1995; Fraser and Swinney 1986) between components of the vector.

Considering the measurements $v(n)$ and $v(n+T)$ as two sets of observations $\mathbf{A} = \{a_i\} = \{v(n)\}$ and $\mathbf{B} = \{b_j\} = \{v(n+T)\}$, the average mutual information $I(T)$, in bits, between these two sets as a function of the time lag T is defined by Fraser and Swinney (1986) and Gallager (1968)

$$I(T) = \sum_{a_i, b_j} P_{AB}(a_i, b_j) \log_2 \left[\frac{P_{AB}(a_i, b_j)}{P_A(a_i) P_B(b_j)} \right], \tag{2.2}$$

where $P_A(a_i)$ is the normalized distribution of measurements from set **A** or the $v(n)$, $P_B(b_j)$ is the normalized distribution of measurements from set **B** or the $v(n+T)$, and $P_{AB}(a_i, b_j)$ is the normalized joint distribution of the two sets of measurements.

For the data from the isolated neuron taken from the STG CPG whose time traces were seen in Figure 1c, we have in Figure 4a the average mutual information $I(T)$. It has become a useful and workable prescription to select the time lag corresponding to the first minimum in $I(T)$ to be for the construction of the data vectors $\mathbf{y}(n)$. From the figure we see that the first minimum is at $T = 9$ ms.

To determine the number of coordinates required to unfold the geometry of the neuronal attractor, we need to ask in what dimension d_E used in the data vectors $\mathbf{y}(n)$ we no longer have overlaps of strands of the orbits because of projection from a higher dimension. In other words, we wish to know when a data point $\mathbf{y}(n)$ has neighbors associated with dynamics rather than with an incorrect and too small choice of dimension in which to view the data. The method of false nearest neighbors (Kennel *et al.* 1992; Abarbanel *et al.* 1993; Abarbanel 1995) directly answers this question by inquiring when the nearest neighbor of each data point $\mathbf{y}(n)$ in the full data set remains a nearby point when the dimension of the data vector is increased. When this number of true neighbors is 100 percent, we have unfolded the geometry of the dynamics. Additional dimensions for the data space are not required.

This criterion is implemented by asking about the percentage of false nearest neighbors; in Figure 4b we see this statistic as evaluated for the time series observed for the intracellular voltage in the isolated STG neuron. We see clearly that at dimension four or five, the number of false neighbors is nearly zero, and remains nearly zero as dimension is increased. A close examination of the residual percentage of false nearest neighbors shows it levels off near 0.75%, characteristic of slightly noisy measurements. This residual noise level is consistent with the environmental status of the experiment.

The analysis has thus established that the dynamics of the isolated neuron can be captured in four dimensions. This is a global statement. It may be that the dynamics actually lies in a lower dimensional space, but because of the twisting and folding of the trajectory due to the nonlinear processes, the global space required to undo this twisting and folding

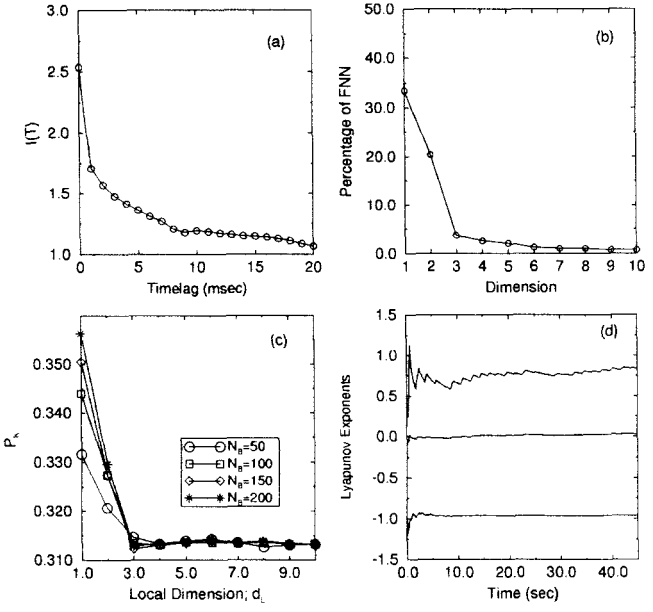

Figure 4: (a) The average mutual information as defined by equation 2.2 for the observations of intracellular voltage in a single neuron from the lobster STG CPG. The first minimum of this is shallow and is located at $T = 9$ ms. (b) Global false nearest neighbors for the intracellular voltage observations on a single neuron from the lobster STG CPG. The percentage of false nearest neighbors essentially reaches zero at global embedding dimension $d_E = 4$. There is some residual in this statistic for dimensions greater than this reflecting high-dimensional contamination (i.e., noise). (c) Local false nearest neighbors for the intracellular voltage observations on a single neuron from the lobster STG CPG. The percentage of bad predictions P_K becomes independent of local dimension d_L and of the number of neighbors used to make local predictions at $d_L = 3$. (d) Lyapunov exponents for the single LP neuron from the lobster STG CPG. We worked in $d_E = d_L = 3$ and used time lag $T = 9$ suggested by average mutual information. The system exhibits one positive Lyapunov exponent, one zero exponent indicating that differential equations govern the data, and one negative exponent.

is larger than the local dynamics in this space. To establish if this is the case, we utilize the test of local false nearest neighbors (Abarbanel and Kennel 1993; Abarbanel 1995), which asks what is happening locally on the attractor and does so in a space larger than or equal to the dimension established in the global false nearest neighbors test. Here this means

looking in global dimension five or greater to see what local dimension of the dynamics captures the variation of the data. We have examined the STG isolated neuron data in global dimension $d_E = 12$ to give us a long region of dimensions in which the local false neighbors can show independence of dimension and of number of neighbors. We know that for any global dimension greater than five or six, the number of global false neighbors is zero, so any working dimension for local false neighbors greater than this will do. In practice, it is useful to choose the working dimension somewhat larger than the known unfolding dimension. Then we ask, as a function of local dimension d_L and number of neighbors N_B, how well a local polynomial predictor from the neighborhood around data point $\mathbf{y}(i)$ produces the observed points in the neighborhood around $\mathbf{y}(i+1)$. When the number of false predictions P_K as shown in Figure 4c becomes independent of d_L and N_B, we have determined a local dimension for the dynamics. In Figure 4c we see that $d_L = 3$ is selected by the data. This implies that we can make models of the behavior of this isolated neuron with three degrees of freedom. (More details on local dynamical dimension can be found in Abarbanel 1995 and Abarbanel *et al.* 1993.)

A final question we will address concerning the possibility of chaos in the observed behavior of the isolated STG neuron regards the global Lyapunov exponents (Abarbanel *et al.* 1993; Abarbanel 1995; Oseledec 1968), which characterize the stability of orbits when slight perturbations are made to them. Chaotic behavior is established by the presence of one or more positive global Lyapunov exponents. In Figure 4d we show the Lyapunov exponents for the isolated STG neuron as a function of the number of time steps. From this we can see that there is one positive global Lyapunov exponent for this neuron, one zero exponent that tells us that ordinary differential equations govern the behavior of this system, and one negative exponent. A fractal dimension (Abarbanel *et al.* 1993; Abarbanel 1995) can be established from these global exponents; it is ≈ 2.75.

With these analyses in place, we have understood that the dynamics of this neuron are chaotic. The key element in this was our evaluation of the global Lyapunov exponents of the dynamics represented by the measured intracellular voltage trace in the reconstructed phase space using time delays of the measurements. A positive global Lyapunov exponent is the hallmark of chaotic behavior in a dynamical system (Abarbanel 1995).

2.1.3 Chaotic Neurons. The evidence we have presented for chaotic behavior in observed neuron activity is another example of low-dimensional chaos in neurons, which goes along with many other confirmations of this phenomenon. Hayashi and Ishizuka (Hayashi and Ishizuka 1992) describe in detail a series of experiments on a molluscan pacemaker neuron, which shows that when certain levels of current are injected into the neuron, chaotic-appearing behavior is seen. The analysis of that ex-

periment used tools such as Poincaré sections and phase-space portraits, which are convincing but not quantitative. The observations of Hayashi and Ishizuka were on isolated neurons as in the observations we report here. Mpitsos *et al.* (1988) also present evidence for chaotic activity in *Pleurobranchaea californica* using phase-space portraits and a computation of the correlation dimension from their observations. The neurons in the study of Mpitsos *et al.* were not isolated but were part of intact circuits.

We agree with Hayashi and Ishizuka (1992) in their conclusion that chaotic oscillations in neurons are expected to be a normal state of neural activity. Indeed, when one considers the genericity of chaos (Guckenheimer and Holmes 1983) in dynamical systems described by three or more ordinary differential equations coupled with the numerous ion channels operating in neural behavior, one should anticipate chaotic oscillations as the normal state of activity.

2.2 Individual Rose and Hindmarsh Model Neurons. The model neuron we adopt here is familiar and has been explored extensively in the papers of Rose and Hindmarsh (Hindmarsh and Rose 1984; Rose and Hindmarsh 1985) and many subsequent analyses of their models. We will use a three-variable model that describes in dimensionless units the membrane potential $x(t)$ and auxiliary variable called $y(t)$ representing a set of fast ion channels connected with aspects of potassium and sodium transport, and finally a "slow" variable $z(t)$, which captures the slower dynamics of yet other ion channels. It is not our intention to repeat in any detail either the RH analysis and that of others in establishing the basis of this model nor to repeat the analyses of others on the features of this model as a description of neuron activity. This model generates time series that look like the time series of an isolated LP neuron (Fig. 1c), and its strange attractor has the same topology as the one depicted in Figure 3c. Instead, our starting point is that this model contains the appropriate mix of slow and fast dynamics to describe adequately the bursting and spiking behavior of observations in neural systems, and we shall discuss at some length in subsequent sections the interesting and fascinating phenomena that transpire when these model neurons are coupled together.

First we establish some general aspects of the RH model that satisfy the differential equations

$$\begin{aligned} \frac{dx(t)}{dt} &= y(t) + \phi(x(t)) - z(t) + I, \\ \frac{dy(t)}{dt} &= \psi(x(t)) - y(t), \\ \frac{dz(t)}{dt} &= -rz(t) + rS(x(t) - c_x). \end{aligned} \tag{2.3}$$

where the two functions $\phi(x)$ and $\psi(x)$ are determined from empirical observations on voltage current relations. The choice suggested by Rose

and Hindmarsh varies with the system they are describing in detail, but the following are conventional:

$$\begin{aligned} \phi(x) &= ax^2 - x^3, \\ \psi(x) &= 1 - bx^2, \end{aligned} \tag{2.4}$$

where $a = 3$ and $b = 5$. Similarly the linear appearance of the membrane voltage in the governing equation for the slow variable $z(t)$ is discussed at length by Hindmarsh and Rose. For some situations they choose an exponential dependence on membrane voltage for this term, but we have settled on the simpler linear description. It is our experience with this system that although details do depend on the functional choices, the basic features operating in the communication between and synchronization of neurons are not dependent on much beyond the appearance of slow and fast subsystems as featured in the model we adopt. The other parameters in the equations are chosen in our calculations as the injected current $I = 3.281$, the voltage $c_x = -1.6$, the scale of the influence of the membrane voltage on the slow dynamics $S = 4.0$, and the time scale for the slow adaptation current r we choose as $r = 0.0021$.

Little, if anything, in our analysis of synchronized behavior of these model neurons depends on the specific values of these parameters. This choice does result in chaotic behavior. To see this we display in Figure 5 two samples of the same time series from the solution of these equations. The equations were solved with a very fine time step using a fourth-order Runge-Kutta scheme. This solution oversampled the waveforms but ensured that all interesting variation in the dynamics would be represented. The output from the solution was desampled to produce a dimensionless time step $\Delta t = 1.0$ to produce the displays in Figure 5.

Many key features of this model are captured in the simple properties of the vector field (the right-hand side) of equation 2.3 in the case when $z(t)$ is ignored. We then have three equilibrium points and a stable limit cycle on the $(x(t), y(t))$ phase plane. These are shown in Figure 6. The stable separatrix of the equilibrium saddle point, labeled RS for resting state in Figure 6, is the basin boundary for the limit cycle. When one changes the initial condition for this reduced model or equivalently adds a short impulse through the synaptic current I, it is possible to bump the system behavior from one attractor, namely, the stable equilibrium point, to the other attractor, namely, the stable limit cycle. If we hold the slow variable z at zero, then when the model neuron is properly triggered, it can enter an indefinitely long period of repetitive firing; this is just the limit cycle behavior.

When the slow dynamics is turned on, however, the repetitive firing can cease, and the neuron will return to its resting state. This resting state corresponds to the saddle node RS. After a relaxation time of order $\frac{1}{r}$, the system may move back to $z \approx 0$, and the repetitive firing will resume. As it resumes, depending on the system parameters, one will see regular firing, namely, periodic motions, or chaotic time traces.

3 Synaptic Coupling of Two RH Neurons

3.1 Electrical Coupling. We now turn our attention to the behavior of two of our model neurons when they are coupled. Three kinds of coupling are of interest here. The first is a simple electrical coupling that treats the channel between the neurons as a wire with no structural

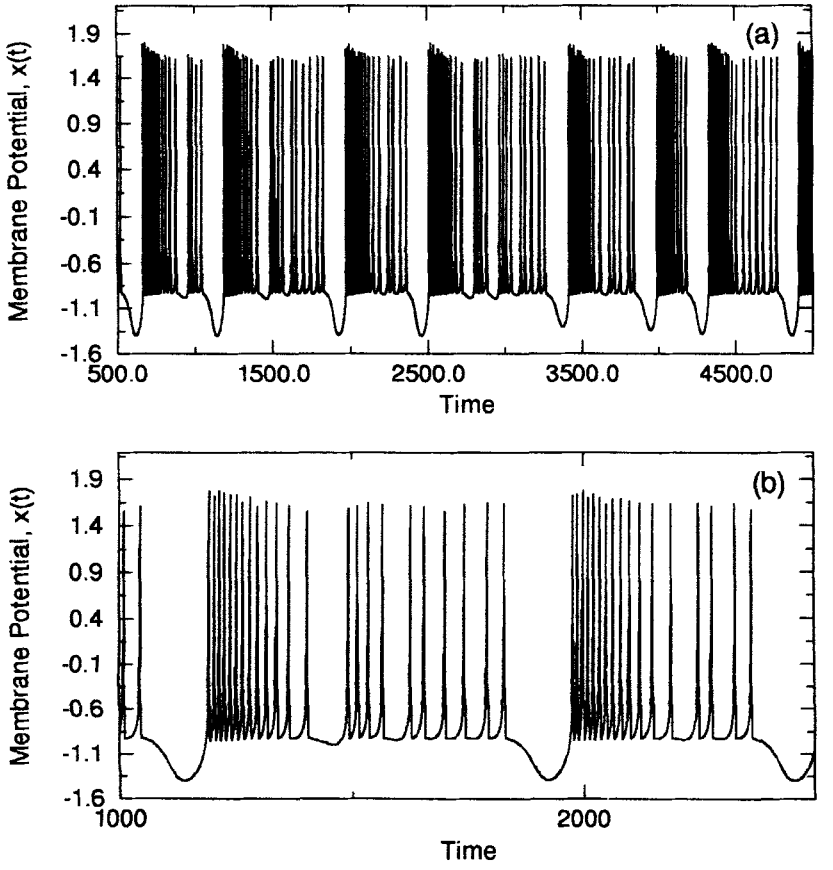

Figure 5: (a) Times series from our model neuron, equation 2.3, with parameters $I = 3.281$. $S = 4.0$. $c_x = -1.6$, and $r = 0.0021$. (b) Blowup of part of the previous time series from the RH neuron.

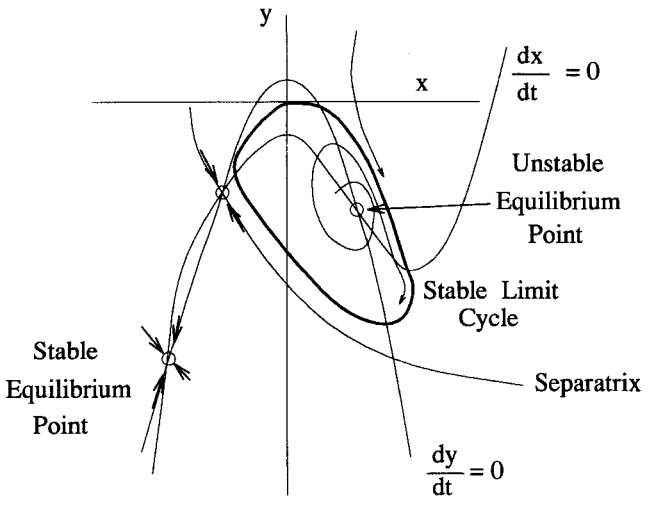

Figure 6: The nullclines of the RH model.

properties. We model this electrotonic coupling as

$$\begin{aligned}
\frac{dx_1(t)}{dt} &= y_1(t) + \phi(x_1(t)) - z_1(t) + I \\
&\quad -(\epsilon + \eta(t))(x_1(t) - x_2(t)), \\
\frac{dy_1(t)}{dt} &= \psi(x_1(t)) - y_1(t), \\
\frac{dz_1(t)}{dt} &= -rz_1(t) + rS(x_1(t) - c_x), \\
\frac{dx_2(t)}{dt} &= y_2(t) + \phi(x_2(t)) - z_2(t) + I \\
&\quad -(\epsilon + \eta(t))(x_2(t) - x_1(t)), \\
\frac{dy_2(t)}{dt} &= \psi(x_2(t)) - y_2(t) \\
\frac{dz_2(t)}{dt} &= -rz_2(t) + rS(x_2(t) - c_x).
\end{aligned} \tag{3.1}$$

These are two identical model neurons of the form discussed above coupled with a parameter ϵ, which is a conductance for the "wire" connecting them. The quantity $\eta(t)$ is gaussian, white noise which has zero

mean and RMS amplitude σ. We add this noise term, which we restrict to a very small amplitude, for two reasons:

1. All laboratory measurements are noisy. To provide a simple source for this continual perturbation of our coupled systems, we have placed these nondeterministic or high-dimensional fluctuations in the coupling mechanism among the chaotic neurons.
2. When one couples together model neurons with three degrees of freedom each, the total possible phase space can become both quite large and rich in fine structure and details of basin boundaries in phase space, which, since all measurements are really noisy, we have no chance of observing in the laboratory. To smooth out these complex details, we attribute some noise to the coupling among neurons. We could have attributed the noise to the individual neurons themselves and accomplished essentially the same goal.

This electrical coupling has been well studied in the physical sciences literature (Fujisaka and Yamada 1983; Afraimovich *et al.* 1986; Rulkov *et al.* 1992), and it is known that it often possesses a submanifold of the full six-dimensional phase space where

$$x_1(t) = x_2(t), \quad y_1(t) = y_2(t), \quad \text{and } z_1(t) = z_2(t). \tag{3.2}$$

On this submanifold we clearly have identical chaotic oscillations of the two neuron oscillators, for on this manifold the coupling term is precisely zero and the individual dynamics is just the same as if the neurons were not coupled at all. When the submanifold is stable, that is, it is an attractor, the neurons are synchronized yet chaotic.

We can show that the synchronization of chaotic motions will occur with certainty if the coupling ϵ is strong enough. To see that, introduce the difference variables for the coupled system

$$\begin{aligned} v(t) &= x_1(t) - x_2(t). \\ u(t) &= y_1(t) - y_2(t) \\ w(t) &= z_1(t) - z_2(t). \end{aligned} \tag{3.3}$$

representing the distance from the submanifold. When $\eta(t) = 0$, the equations governing $u(t)$, $v(t)$, and $w(t)$ are

$$\begin{aligned} \frac{dv(t)}{dt} &= u(t) - (a(x_1(t) + x_2(t)) - (x_1^2(t) + x_2^2(t) \\ &\quad + x_1(t)x_2(t)) + 2\epsilon)v(t) - w(t) \\ \frac{du(t)}{dt} &= -b(x_1(t) + x_2(t))v(t) - u(t) \\ \frac{dw(t)}{dt} &= -rw(t) + rSv(t). \end{aligned} \tag{3.4}$$

with $a = 3.0$, and $b = 5.0$.

If we consider the function

$$L(t) = \frac{v(t)^2}{2} + \frac{2au(t)^2}{b^2} + \frac{w(t)^2}{2rS}, \tag{3.5}$$

then from the equations of motion we find

$$\begin{aligned}\frac{dL(t)}{dt} &= -\varphi(\epsilon,t)v(t)^2 - \frac{[8u(t) - b^2v(t) + 4bv(t)(x_1(t) + x_2(t))]^2}{16ad^2} \\ &\quad -\frac{w(t)^2}{S},\end{aligned} \tag{3.6}$$

with

$$\varphi(\epsilon,t) = 2\epsilon + 3x_1(t)x_2(t) + \left(\frac{b}{2} - a\right)(x_1(t) + x_2(t)) - \frac{b^2}{16}. \tag{3.7}$$

When $\varphi(\epsilon,t) > 0$, then $L(t)$ will be a Lyapunov function for the coupled system of neurons. In this case both the fixed point $(v(t),u(t),w(t)) = (0,0,0)$ and the submanifold above will be stable for any initial condition. This translates to the statement that synchronized motions are ensured when

$$2\epsilon > \max\left\{-3x_1(t)x_2(t) - \left(\frac{b}{2} - a\right)(x_1(t) + x_2(t)) + \frac{b^2}{16}\right\}. \tag{3.8}$$

In the Appendix we show that all trajectories in the full six-dimensional space of the coupled neurons move in a bounded domain of the full space and cannot depart from it. This means that for large enough ϵ, the synchronization condition is certainly satisfied.

Now we look at some numerical evidence for synchronized behavior of these model neurons with electrotonic coupling. We set the root mean square (RMS) level of the white noise at $\sigma = 0.005$. To exhibit the synchronization, we introduce two useful measures of the "distance" between the neuron activity. In these measures of distance, we concentrate on the connection between the membrane potentials $x_1(t)$ and $x_2(t)$ in the neurons. Since the neurons are identical, it is sufficient to examine this connection.

3.1.1 "Distances" Between the Coupled Neurons. The first distance measure is essentially the RMS difference between the $x_1(t)$ motion, and the $x_2(t)$ motion, with the difference that we recognize from the outset that a shift in the timing of the chaotic motions of the two neurons may occur due to the coupling. To allow for this, we define the average distance $D(\tau,\epsilon)$ between the two neural behaviors as

$$D^2(\tau,\epsilon) = \frac{1}{N_s}\sum_{k=1}^{N_s}(x_1(k) - x_2(k+\tau))^2, \tag{3.9}$$

where τ is the possible time shift needed to "align" the two neurons and N_s is the total number of samples.

To distinguish between the bursting and spiking motions and examine the synchronization in the bursting alone, we delimit the values of $x_i(t)$ by replacing any values greater than -1 with -1. This eliminates the spikes and retains the bursts in the membrane potential. A high-pass filtering of the data would achieve the same end. When this delimiting is employed, we call the average distance the bursting average distance $DB(\tau, \epsilon)$.

In characterizing the synchronization, we have examined the $D(\tau, \epsilon)$ and $DB(\tau, \epsilon)$ as a function of the coupling ϵ at that value of τ for which each distance measure is minimum. This is nothing but tracking along the valley of minimum values of $D(\tau, \epsilon)$ or $DB(\tau, \epsilon)$ and labeling the location along that valley by ϵ. In Figure 7a we show $D(\tau_{min}, \epsilon)$, which is the RMS distance as defined above for the time shift τ_{min}, which at fixed coupling ϵ yields the minimum value of $D(\tau, \epsilon)$. It is clear that for ϵ just a bit bigger than 0.5 and in a region about $\epsilon \approx 0.2$, the neurons appear synchronized. In Figure 7b we have $DB(\tau_{min}, \epsilon)$, which exhibits more or less the same characteristics as $D(\tau_{min}, \epsilon)$ but also suggests that some synchronization among the slow or bursting motions of the neurons may be appearing near $\epsilon \approx 0.04$.

A third characteristic is achieved by looking at the time shifts τ_{min}, which minimize $DB(\tau, \epsilon)$ at each ϵ. This function $\tau_{min}(\epsilon)$ is shown in Figure 7c. This reveals an interesting new possibility for the synchronized neurons. For couplings in the neighborhood of $\epsilon \approx 0.2$, we see that synchronization of the bursts is reached with a nonzero τ_{min}, which is nearly the same for a range of ϵ. The synchronization for other values of ϵ is reached with $\tau_{min} \approx 0$. For $\epsilon \approx 0.2$ this suggests that the electrically coupled neurons are synchronized but out of phase with each other. This is quite different from the synchronization on the submanifold discussed above, which we know is reached for large ϵ. The same phenomenon for "limit-cycle" neuron models has been discussed over the past few years (Sherman and Rinzel 1992; Han *et al.* 1995). Here we have a more general case: regularization of chaos and antiphase locking for electrically coupled chaotic oscillators.

Looking now at the time traces of $x_1(t)$ and $x_2(t)$ for $\epsilon \approx 0.2$ we can see in Figure 8 visual evidence of the various kinds of phase synchronization. Figure 9a shows the out-of-phase synchronization that occurs when $\epsilon \approx 0.2$. In Figure 9b we have $\epsilon \approx 0.4$ and see evidence of a partial synchronization of the two coupled HR neurons. When we raise ϵ to 0.8, as in Figure 9c, we see full synchronization of the two model neurons.

3.1.2 Mutual Information Between Two Coupled Neurons. The key question we are addressing in this paper is the level of synchronization between two chaotic neurons in order to organize them for directed collective behavior. To examine synchronization from this point of view, we

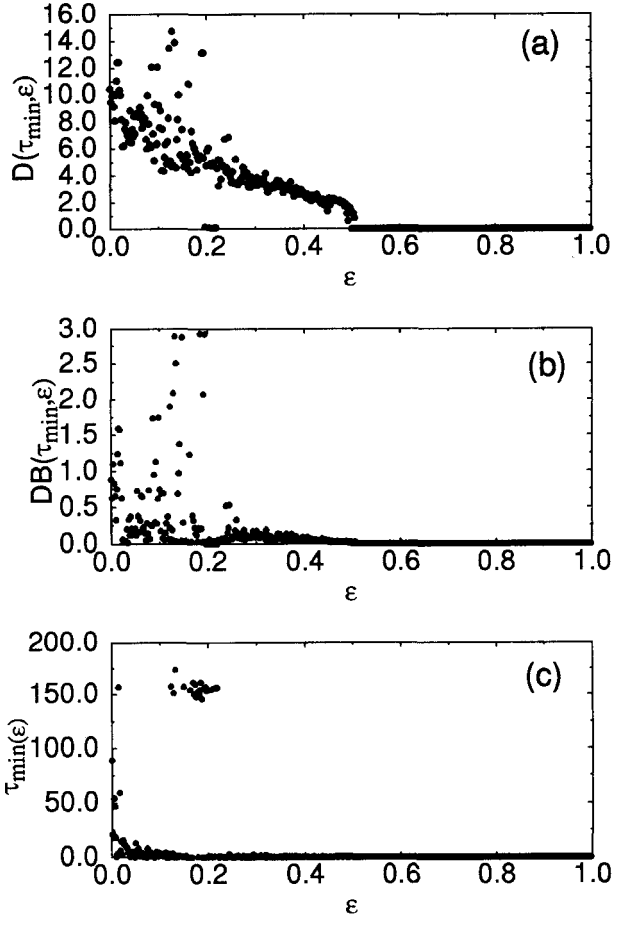

Figure 7: (a) The distance statistic, equation 3.9, for electrically coupled RH neurons. The RMS noise level introduced into the coupling is $\sigma = 0.005$. Near $\epsilon \approx 0.2$ and for $\epsilon \geq 0.5$ the model neurons are synchronized. (b) The bursting distance statistic for electrically coupled RH neurons. The RMS noise level introduced into the coupling is $\sigma = 0.005$. Near $\epsilon \approx 0.2$ and for $\epsilon \geq 0.5$ the model neurons are synchronized. (c) The time at which the distance statistic, equation 3.9, is a minimum as a function of ϵ. The synchronization near $\epsilon \approx 0.2$ apparent in Figure 12 requires a large time delay and is antiphase synchronization. The synchronization for $\epsilon \geq 0.5$ is in phase.

now evaluate the average mutual information between measurements of the membrane potential in the first neuron $x_1(t)$ and the membrane po-

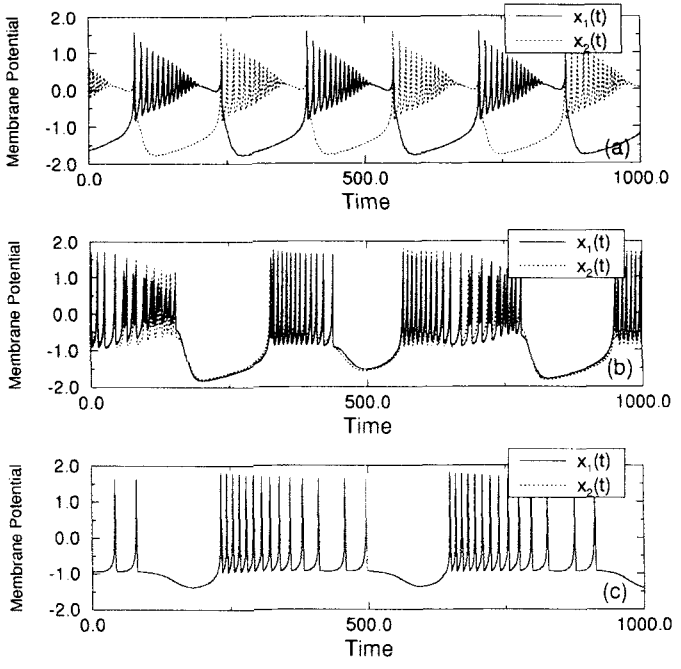

Figure 8: (a) Membrane potentials $x_1(t)$ and $x_2(t)$ from electrically coupled RH neurons for $\epsilon = 0.2$ The synchronization is antiphase. (b) Membrane potentials $x_1(t)$ and $x_2(t)$ from electrically coupled RH neurons for $\epsilon = 0.4$ The synchronization is not complete but nearly in phase. (c) Membrane potentials $x_1(t)$ and $x_2(t)$ from electrically coupled RH neurons for $\epsilon = 0.4$ The synchronization is complete and in phase.

tential in the second neuron $x_2(t+\tau)$ at some time lag τ between the measurements. To evaluate the average mutual information from the measurements $x_1(t)$ and $x_2(t)$, we bin the data into M bins by defining discrete variables $s_1(n)$ and $s_2(n)$ through

$$\begin{aligned} x_j(n) < -2 \text{ then } s_j(n) &= h_0 \\ -2 + 4\frac{k-1}{M-1} \leq & \\ x_j(n) < -2 + 4\frac{k}{M-1} \text{ then } s_j(n) &= h_k,\ k = 1, \ldots, M-2 \\ x_j(n) \geq 2 \text{ then } s_j(n) &= h_{M-1}. \end{aligned} \tag{3.10}$$

where $h_0, h_1, \ldots, h_{M-1}$ are any set of M "letters" designating bins for the values of the $x_j(n)$. Using this binning of the data for membrane potential

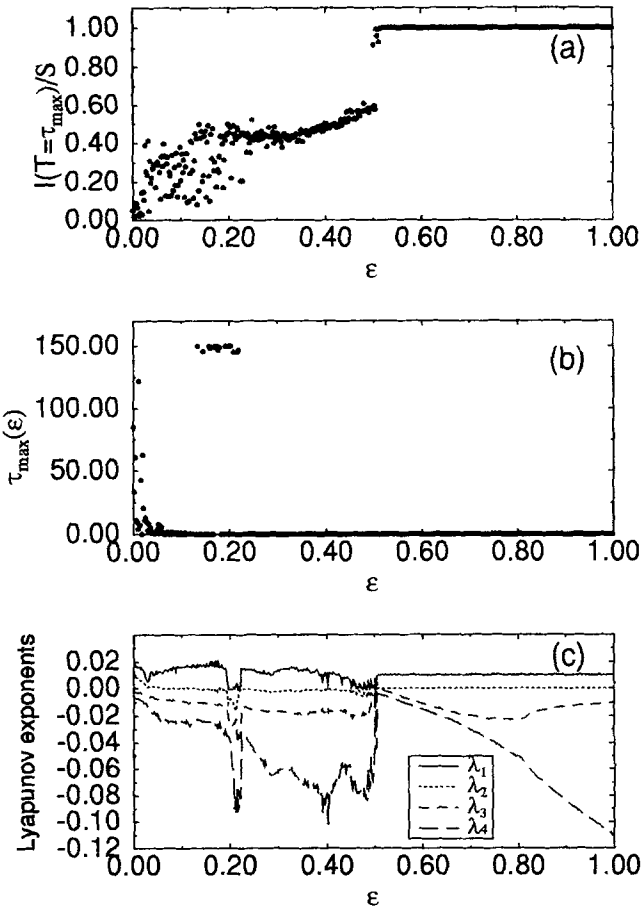

Figure 9: (a) The average mutual information at the time delay where it is a maximum as a function of the coupling ϵ for electrically coupled RH neurons. The average mutual information is normalized by the entropy of the individual neurons. (b) The time $\tau_{\max}(\epsilon)$ at which the average mutual information between electrically coupled RH neurons is a maximum. The antiphase synchronization for $\epsilon \approx 0.2$ and the in-phase synchronization for $\epsilon \geq 0.5$ are revealed here. (c) The four largest Lyapunov exponents for the electrically coupled RH neurons as a function of the coupling strength ϵ. These are evaluated directly from the equations of motion. When we have antiphase synchronization near $\epsilon \approx 0.2$, the system is not chaotic since all $\lambda_a \leq 0$. For $\epsilon \geq 0.5$, the coupled system is chaotic as one of the exponents is positive.

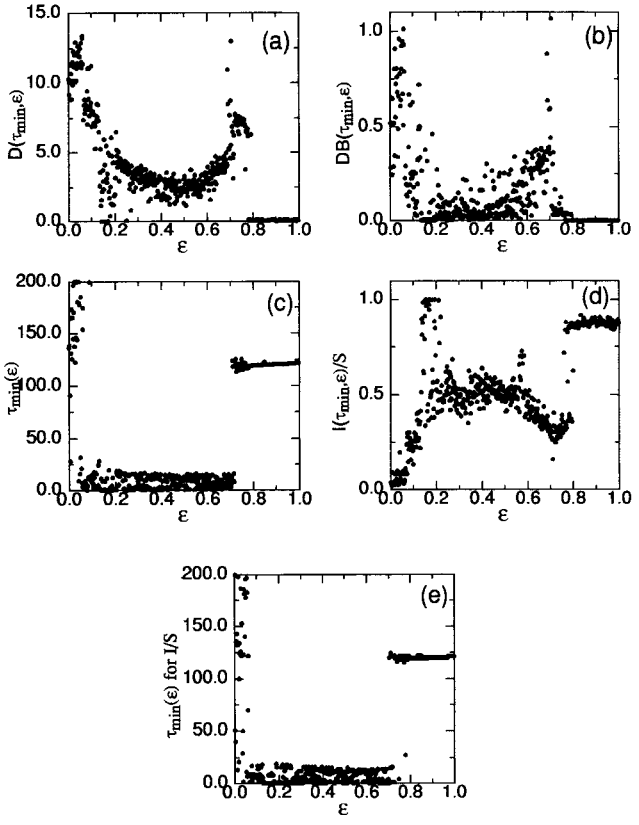

Figure 11: (a) The distance statistic for inhibitory coupling between RH neurons. The RMS noise level introduced into the coupling is $\sigma = 0.005$. Near $\epsilon \approx 0.17$ and for $\epsilon \geq 0.8$ the model neurons are synchronized. (b) The bursting distance statistic for inhibitory coupling between RH neurons. Near $\epsilon \approx 0.2$ and for $\epsilon \geq 0.8$ the model neurons are synchronized. (c) The time at which the distance statistic is a minimum as a function of ϵ. The model RH neurons are coupled by inhibitory synaptic coupling. The synchronization near $\epsilon \approx 0.2$ is in phase and for $\epsilon \geq 0.8$ is antiphase. (d) The average mutual information at the time delay where it is a maximum as a function of the coupling ϵ for inhibitory coupling between RH neurons. The average mutual information is maximal for the in-phase synchronization, which occurs for $\epsilon \geq 0.8$ and for $\epsilon \approx 0.2$. (e) The time $\tau_{max}(\epsilon)$ at which the average mutual information between RH neurons coupled with inhibitory synaptic coupling is a maximum. The antiphase synchronization for $\epsilon \geq 0.8$ and the in-phase synchronization for $\epsilon \approx 0.2$ *are seen here.*

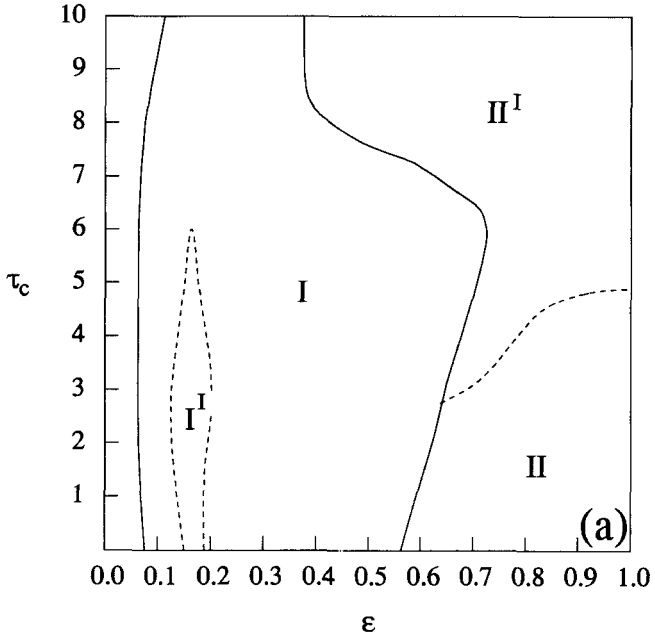

Figure 10: (a) The "phase" diagram for inhibitory coupling between the coupled RH neurons as a function of the coupling strength ϵ and the time delay τ_c in the synaptic coupling. The four labeled regions correspond to different types of synchronization illustrated by the time traces in the next figures.

to a time delay in the action of one neuron on another. We choose to represent this as a response in the membrane potential of one neuron that is delayed and subject to a threshold over which the potential must rise along with that delay. In the equation for the membrane potential of neuron 1, $x_1(t)$, for example, we will add a response associated with the behavior of neuron 2's potential $x_2(t)$ of the form

$$-(\epsilon + \eta(t))(x_1(t) + V_c)\theta(x_2(t - \tau_c) - X). \tag{3.14}$$

where, as above, ϵ is the strength of the coupling and $\eta(t)$ is a very small zero mean noise term with RMS magnitude σ. The new ingredients in this coupling term are the thresholding associated with the Heaviside function $\theta(w)$, which is unity for $w > 0$ and vanishes for $w < 0$. In addition, we have a reverse potential V_c, which tells us the magnitude of the response to the threshold, and we have a threshold X over which the other neuron's membrane potential must have rise at a time delayed

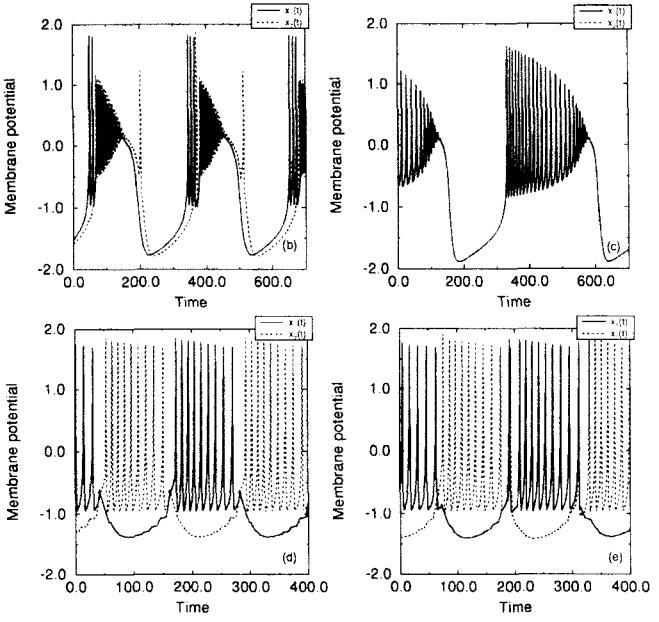

Figure 10: *Continued.* (b) Membrane potentials $x_1(t)$ and $x_2(t)$ from RH neurons with inhibitory coupling in Region I. $\tau_c = 4.0$. The synchronization is nearly complete and in phase. (c) Membrane potentials $x_1(t)$ and $x_2(t)$ from RH neurons with inhibitory coupling in Region I'. $\tau_c = 4.0$. The synchronization is complete and in phase. (d) Membrane potentials $x_1(t)$ and $x_2(t)$ from RH neurons with inhibitory coupling in Region II. $\tau_c = 4.0$. The synchronization is complete and antiphase. (e) Membrane potentials $x_1(t)$ and $x_2(t)$ from RH neurons with inhibitory coupling in Region II'. $\tau_c = 4.0$. The synchronization is complete and antiphase.

by τ_c. The response to potential $x_1(t)$ on the part of $x_2(t)$ will simply have $1 \rightarrow 2$ in the coupling term. Inhibitory coupling of the neurons is associated with a reverse potential $V_c > 0$, while we achieve excitatory coupling by choosing $V_c = 0.0$. The threshold potential we choose as $X = 0.85$ in each case.

This section considers the result of inhibitory coupling. We have the six differential equations among the membrane potentials and the fast and slow auxiliary variables:

$$\begin{aligned}\frac{dx_1(t)}{dt} &= y_1(t) + \alpha(x_1(t)) - z_1(t) + I \\ &\quad - (\epsilon + \eta(t))(x_1(t) + V_c)\theta(x_2(t - \tau_c) - X),\end{aligned}$$

$$
\begin{aligned}
\frac{dy_1(t)}{dt} &= \psi(x_1(t)) - y_1(t), \\
\frac{dz_1(t)}{dt} &= -rz_1(t) + rS(x_1(t) - c_x), \\
\frac{dx_2(t)}{dt} &= y_2(t) + \phi(x_2(t)) - z_2(t) + I \\
&\quad - (\epsilon + \eta(t))(x_2(t) + V_c)\theta(x_1(t - \tau_c) - X), \\
\frac{dy_2(t)}{dt} &= \psi(x_2(t)) - y_2(t) \\
\frac{dz_2(t)}{dt} &= -rz_2(t) + rS(x_2(t) - c_x), \qquad (3.15)
\end{aligned}
$$

and we use the parameters $\sigma = 0.005$. $X = 0.85$, and $c_x = 1.6$ in our work here. $V_c = 1.4$ for the inhibitory coupling. The HR neurons we have coupled in this time-delayed fashion are identical, as embodied in our totally symmetric couplings. We shall not consider asymmetric couplings or coupling differing neurons in this paper, but we plan to return to these cases.

Although there are now six ordinary differential equations representing the coupled behavior of two HR neurons because of the time delay involved in the equations, there are now, using the usual description of degrees of freedom in differential equations, an infinite number of degrees of freedom. The time delay leads via Taylor series of expressions such as $x_1(t - \tau_c)$ to an infinite number of derivatives of $x_1(t)$ appearing in the equations. This means that the phase space or state space of these coupled systems could be very large indeed, but we demonstrate below that the phase space occupied by the solutions to these coupled neurons is in fact quite small.

We have examined the solutions to these coupled equations using the parameters just mentioned, as well as the parameters used above in our discussion of electrical coupling. We are unable to give the same argument via a Lyapunov function that for large enough coupling ϵ we will have synchronization between our identical HR neurons, but synchronization does occur, and we have uncovered it by numerical work. The qualitative aspects of this are displayed in Figure 10a, which is a kind of phase diagram for this system. We indicate the different behaviors seen as we vary both the coupling strength ϵ and the time delay τ_c.

To illustrate further the typical behaviors found in the various regions of (τ_c, ϵ) space, we show in Figure 11b time traces from $x_1(t)$ and $x_2(t)$. The nearly synchronized and nearly in-phase behavior of the two neurons varies little with ϵ within the region denoted I in Figure 10a. The behavior in Region I′ is shown in Figure 10c. Here the two neurons are completely synchronized and fully in phase. Region II is typified by the time traces in Figure 10d. In this region the neurons are completely out of phase but clearly synchronized. Finally Region II′, as seen in Figure 10e,

shows a slight variation on Region II behavior with the first spiking of neuron 1 the last synchronized connection with the spiking of neuron 2, which ends at that point. The distinction between these regions is qualitative only, but these example time evolutions serve to demonstrate the wide range of synchronization phenomena one encounters and which we suggest one may look for in the laboratory.

Next we examine data from the model neurons with inhibitory coupling at a fixed time delay, $\tau_c = 4$, but as a function of coupling strength ϵ. Figure 10a is the distance measure we introduced above, and we can see synchronization based on this statistic in the neighborhood of $\epsilon \approx 0.2$ and for $\epsilon \geq 0.8$. For other values of ϵ there seems to be little synchronization. The bursting distance is displayed in Figure 12b and in an approximate sense is telling us rather similar information to the regular distance $D(\tau_{\min}, \epsilon)$. Figure 12c has the values of $\tau_{\min}(\epsilon)$ for this inhibitory data, and we can see that in-phase synchronization can be associated with $\epsilon \approx 0.2$, while for $\epsilon \geq 0.8$ we have out-of-phase synchronization. This is essentially what the time traces shown above are telling us.

The information measure of synchronization, displayed in Figure 12d for the inhibitory coupling case, tells us that for both $\epsilon \approx 0.2$ and $\epsilon \geq 0.8$ we have high average mutual information between the neurons. Figure 11e, which has the times of maximum mutual information as a function of ϵ, verifies the earlier comments about in-phase and out-of-phase synchronization.

Each of the cases studied across the (τ_c, ϵ) plane has its own intrinsic interest. Our emphasis here is on the qualitative behaviors seen as we visit regions of this parameter plane. In particular, it is important to note that synchronization both in-phase and out-of-phase occurs across large regions of this parameter space.

3.3 Excitatory Coupling. Excitatory coupling of the two neurons is described by the same differential equations as above, but now $V_c = 0.0$. In surveying the (τ_c, ϵ) plane we found three typical kinds of synchronized behavior. Each is nearly fully synchronized motion of both neurons, but the regions differ by the nature of the actual bursting, spiking characteristics. In Figure 12a we see the first of these, which is a rather familiar kind of neuronal activity. This kind of synchrony occurs over the range of coupling $0.05 \leq \epsilon \leq 0.1$. Figure 12b shows another kind of synchronous behavior, which appears in the range $0.1 \leq \epsilon \leq 0.15$. Finally Figure 12c displays synchronized behavior, which results when from $0.15 \leq \epsilon \leq 1.0$. In each of these examples the synchrony is in phase, essentially complete, and results in periodic motion of the coupled neurons.

The distance and information measures for synchronization bear out these qualitative observations. In Figure 13a we have $D(\tau_{\min}, \epsilon)$ for excitatory coupling at $\tau_c = 4$. Clearly for $\epsilon \geq 0.2$ the synchronization is complete and in phase. $DB(\tau_{\min}, \epsilon)$, shown in Figure 13b, for the same

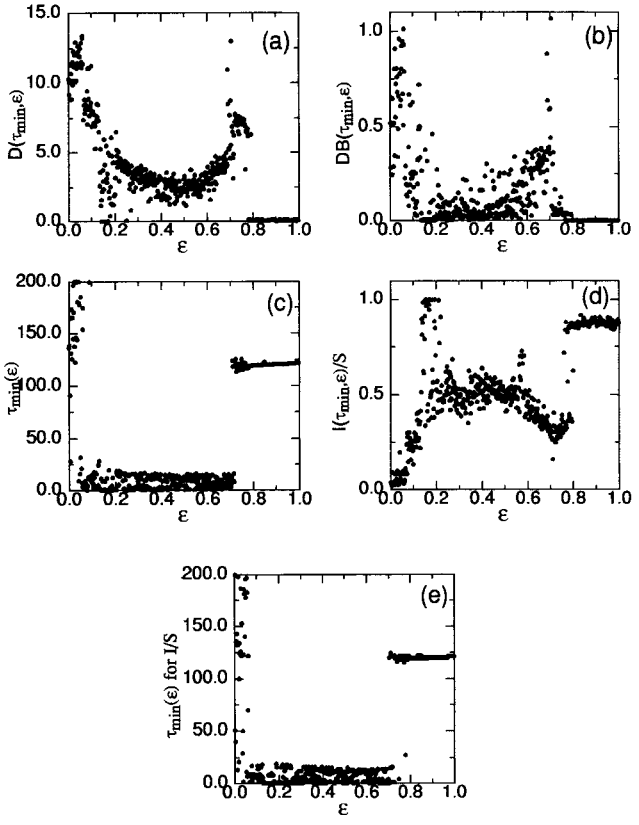

Figure 11: (a) The distance statistic for inhibitory coupling between RH neurons. The RMS noise level introduced into the coupling is $\sigma = 0.005$. Near $\epsilon \approx 0.17$ and for $\epsilon \geq 0.8$ the model neurons are synchronized. (b) The bursting distance statistic for inhibitory coupling between RH neurons. Near $\epsilon \approx 0.2$ and for $\epsilon \geq 0.8$ the model neurons are synchronized. (c) The time at which the distance statistic is a minimum as a function of ϵ. The model RH neurons are coupled by inhibitory synaptic coupling. The synchronization near $\epsilon \approx 0.2$ is in phase and for $\epsilon \geq 0.8$ is antiphase. (d) The average mutual information at the time delay where it is a maximum as a function of the coupling ϵ for inhibitory coupling between RH neurons. The average mutual information is maximal for the in-phase synchronization, which occurs for $\epsilon \geq 0.8$ and for $\epsilon \approx 0.2$. (e) The time $\tau_{max}(\epsilon)$ at which the average mutual information between RH neurons coupled with inhibitory synaptic coupling is a maximum. The antiphase synchronization for $\epsilon \geq 0.8$ and the in-phase synchronization for $\epsilon \approx 0.2$ *are seen here.*

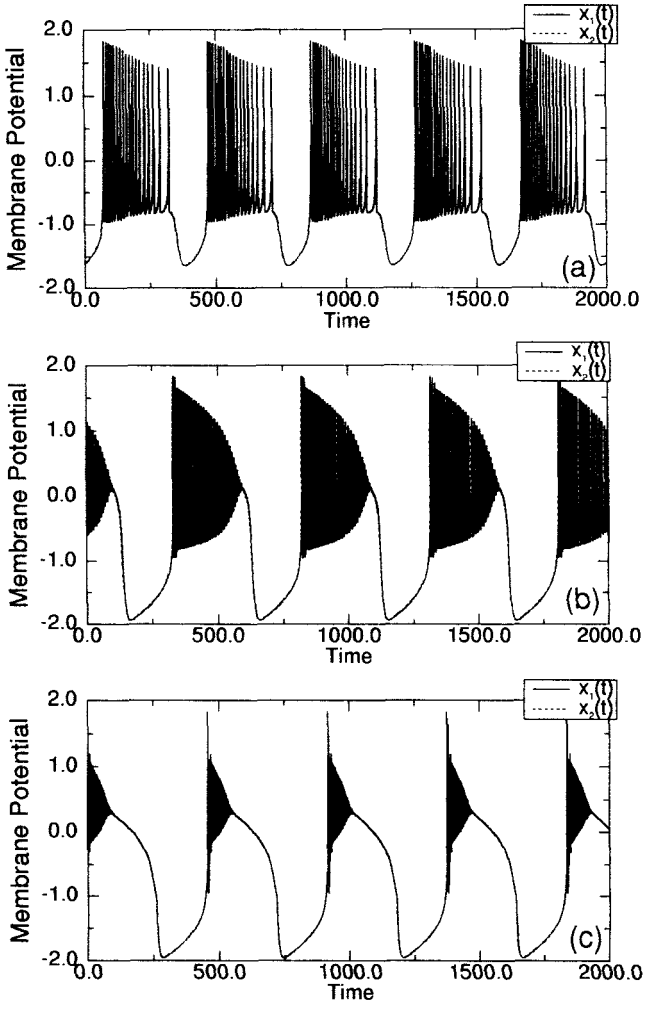

Figure 12: (a) Membrane potentials $x_1(t)$ and $x_2(t)$ from RH neurons with excitatory coupling. $\tau_c = 4.0$ The synchronization is nearly complete and in phase. For this type of synchronization we have $0.05 \leq \epsilon \leq 0.1$. The synchronization results in periodic behavior. (b) Membrane potentials $x_1(t)$ and $x_2(t)$ from RH neurons with excitatory coupling. $\tau_c = 4.0$ The synchronization is nearly complete and in phase. For this type of synchronization we have $0.1 \leq \epsilon \leq 0.15$. The synchronization results in periodic behavior. (c) Membrane potentials $x_1(t)$ and $x_2(t)$ from RH neurons with excitatory coupling. $\tau_c = 4.0$ The synchronization is nearly complete and in phase. For this type of synchronization we have $0.15 \leq \epsilon \leq 1.0$. The synchronization results in periodic behavior.

coupling shows much the same as $D(\tau_{\min}, \epsilon)$. $\tau_{\min}$ confirms the in-phase nature of the synchronization for $\epsilon \geq 0.2$; this is seen in Figure 13c. The information measure of synchronization $I(\tau_{\max}, \epsilon)/S$ is seen in Figure 13d.

4 Discussion and Conclusions

The description of small neural networks behavior like CPGs requires at least the understanding of the cooperative dynamics of minimal neural systems: two synaptically coupled neurons. There are many papers focused on this problem (e.g., Sherman 1994; Sherman and Rinzel 1992; Vreeswijk *et al.* 1994; Skinner *et al.* 1994; Han *et al.* 1995). Nevertheless, all available results related to cooperative behavior of model neurons deal with regular individual dynamics. On the other hand, it is known, and we confirm in our experiments, that the individual dynamics of CPG neurons generates nonregular sequences of spikes on bursts (see Fig. 1). There are some questions raised from this consideration; among them, the main one is to find what mechanisms are responsible for the regular rhythm that achieves muscle control with chaotic neurons in a CPG. The traditional view of electrically coupled chaotic generators is the following: in general, coupled chaotic oscillators generate "hyperchaos," that is, chaos with higher dimension and more complex behavior than for an individual neuron. Only for strong enough coupling can two coupled chaotic generators demonstrate the same chaotic behavior as one. This is chaotic synchronization (Afraimovich *et al.* 1986; Heagy *et al.* 1994). What happens when two chaotic neurons are coupled by synaptic coupling? We addressed this question in this paper and found that two synaptically coupled chaotic neurons order each other and demonstrate regular cooperative dynamics in a broad part of parameter space. Before we discuss the origin of this phenomenon, we have to say a few words about chaotic neural modeling.

A neuron is a nonlinear, nonequilibrium system with several feedbacks. Due to these feedbacks, which open and close ionic channels in the membrane at the various phases of electrical activity, the state of neuron corresponding to the resting potential may became unstable and the neuron oscillates. Such an oscillator acting on the time scale of characteristic period of electric activity $\sim$ 10Hz may be regarded as a dynamical system for which microscopic kinetics acts only as noise. Because the number of different ionic channels is large, it is not really a surprise that real neurons are chaotic oscillators. But the real question is this: Why is it a low-dimensional oscillator? From the mathematical point of view, any generator with noise has an infinite dimension, and the estimation of the dimension depends on the level of description. Nevertheless, when the noise is small, we may distinguish chaotic behavior from noise alone and estimate the number of important degrees of freedom (number of active

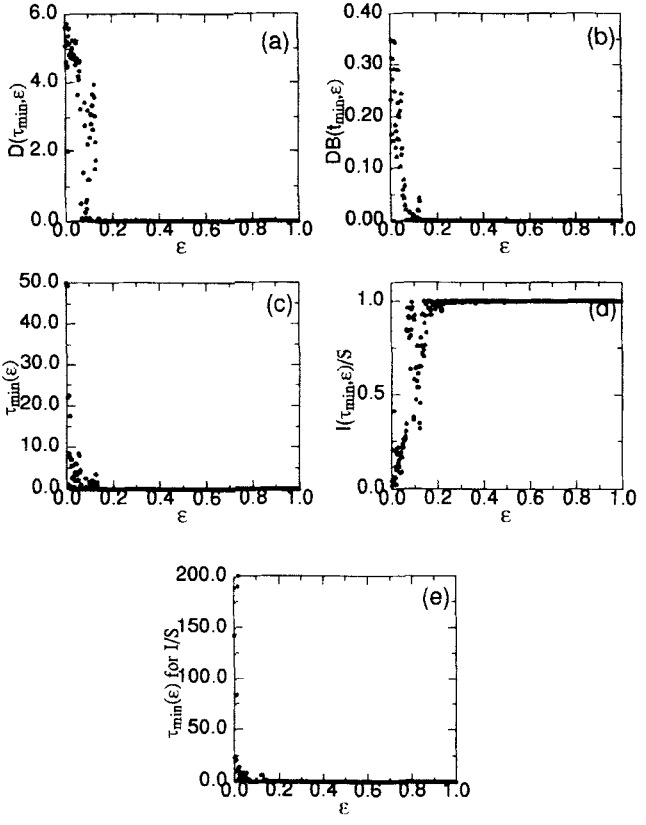

Figure 13: (a) The distance statistic for excitatory coupling between RH neurons. The RMS noise level introduced into the coupling is $\sigma = 0.005$. For $\epsilon \geq 0.15$ the model neurons are synchronized. The synchronized motion is periodic for excitatory coupling. (b) The bursting distance statistic for excitatory coupling between RH neurons. For $\epsilon \geq 0.15$ the model neurons are synchronized. The synchronized motion is periodic for excitatory coupling. (c) The time at which the distance statistic is a minimum as a function of ϵ. The model RH neurons are coupled by excitatory synaptic coupling. The synchronization near $\epsilon \geq 0.15$ is in phase. The synchronized motion is periodic for excitatory coupling. (d) The average mutual information at the time delay where it is a maximum as a function of the coupling ϵ for excitatory coupling between RH neurons. The phase synchronization occurs for $\epsilon \geq 0.15$. The synchronized motion is periodic for excitatory coupling. (e) The time $\tau_{max}(\epsilon)$ at which the average mutual information between RH neurons coupled with excitatory synaptic coupling is a maximum. The synchronization for $\epsilon \geq 0.15$ is in phase. The synchronized motion is periodic for excitatory coupling.

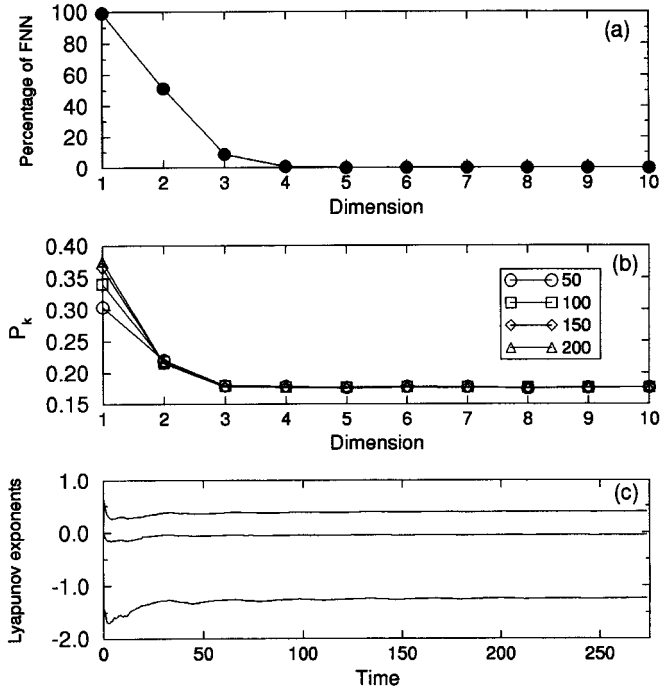

Figure 14: (a) Global false nearest neighbors for the voltage time series from the Rose-Hindmarsh model with 1% noise. The percentage of false nearest neighbors reaches zero at a global embedding dimension $d_E = 4$. (b) Local false nearest neighbors for the voltage time series from the Rose-Hindmarsh model with 1% noise. The percentage of bad predictions P_K becomes independent of the local dimension and of the number of neighbors used to make local predictions at $d_L = 3$. (c) Lyapunov exponents for the same model time series for $d_L = 3$.

independent variables). To do this we used three different approaches: (1) using the observed data, we reconstructed the attractors and examined its variation with changes of applied external current; (2) using the global and local false nearest neighbors, we calculated the embedding dimension and the local dynamical dimension; and (3) we evaluated the Lyapunov exponents. All these results clearly tell us that we may model our CPG neuron by ordinary differential equations with three or four degrees of freedom and small noise.

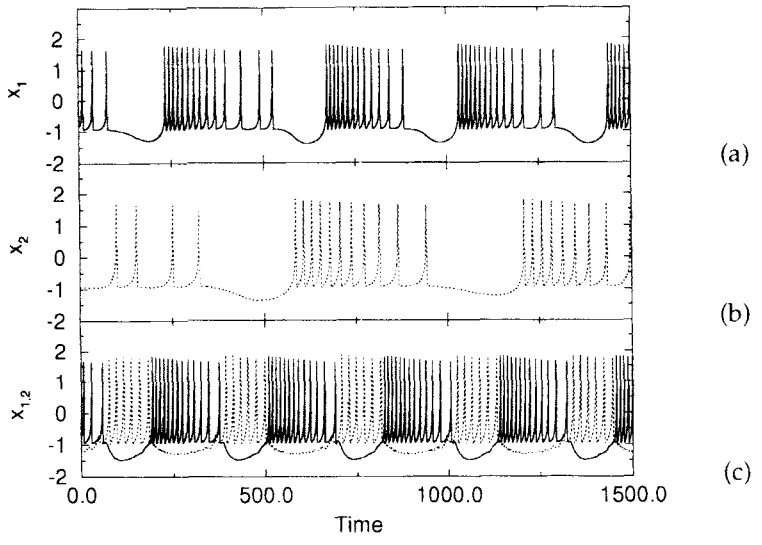

Figure 15: (a,b) Time series of two different RH models. The time scale for the neuron in (a) is half that for the neuron in (b). In (a) $r = 0.0021$ and for (b) $r = 0.0025$. (c) The time course of each of the neurons when they are coupled in a nonsymmetric fashion with reciprocal inhibitory coupling. They are now synchronized and out of phase.

In order to confirm this kind of result on bursting, spiking systems, we performed the same computations on output from our model RH neurons. We introduced small gaussian, white noise with an RMS level of 1% of the model output into the right-hand side of the RH equations. Then we analyzed these data using precisely the same algorithms utilized for the observed data. The results are displayed in Figure 14. We emphasize that the dimension of a strange attractor and the values of the Lyapunov exponents depend strongly on the existence of noise. For example, the positive Lyapunov exponent calculated for the RH model without noise is smaller than the Lyapunov exponent calculated from the voltage time series from the RH model with 1% noise. The origin of this phenomenon is the following: in the phase space of the RH model, there are strong, unstable periodic orbits in the proximity of the attractor, as is clear from the transient time series. When noise is introduced in the system, these unstable orbits become part of the attractor, which leads to an increase of the average Lyapunov exponent. The same occurs in the embedding dimension calculation.

Of course, the RH model is not complete enough for a correct description of every property of spiking-bursting neurons. For example, as formulated, it does not explain the bursting frequency and amplitude of the rebound potential versus current that we can observe in real data (see Fig. 2): (1) the spiking frequency at the beginning of the bursts increases as the applied current decreases, (2) the amplitude of the rebound potential decreases with increasing current; and (3) the interburst frequency increases with current. These properties are important because they determine the cooperative behavior of synaptically coupled bursting neurons. It is possible to generalize the RH model (see Rabinovich *et al.* 1996) to model these features. However, the differences between our new model and the original RH model are not essential when we investigate the cooperative behavior of two identical chaotic neuron models.

These simulations do not provide us with quantitative statements but focus on qualitative behavior as the strength of the coupling is modified. It is not pharmacologically easy to adjust gradually the strength of the coupling. Good experimental support of this mathematical approach can be found matching the qualitative behavior (phase to phase, antiphase, and so on) and the characterization of chaotic motion seen in a few experimental points and the numerical calculations. In our opinion, to be able to make qualitative predictions justifies this work.

A natural objection drawn from these predictions is that the two model neurons are identical, as is the identical reciprocal coupling. This raises the question: Is this predicted qualitative behavior maintained when this symmetry is broken? To answer this question requires an increase in the number of parameters to be explored. We have not made a systematic survey of the parameters as part of the present work, but have explored an example of two RH model neurons with different internal parameters that are coupled reciprocally by inhibitory connections, and these connections have different strengths. The parameters of the RH neurons are set so that they have a time scale of about a factor of two with respect to each other, and the coupling strengths were $\epsilon_1 = 0.6$ and $\epsilon_2 = 1.4$ for the two synapses. In Figure 15a and 15b we have the time courses of the individual model neurons, and it is clear they act rather differently. When they are coupled as indicated, they synchronize, out of phase as it happens (see Fig. 15c). This provides clear evidence that nonidentical neurons with nonsymmetric coupling can synchronize. The synchronization explored at some depth in this paper regarding similar neurons symmetrically coupled can now be seen as one case of a general phenomenon. The robustness of the phenomenon is very important if we are to focus on it as the mechanism for coherent cooperative behavior in networks of neurons that might well be different individually.

Appendix

In this Appendix we show that the stability condition (equation 3.8) is satisfied when the coupling is strong enough. By doing this we prove that all attractors in the six-dimensional phase space of the dynamical system (equation 3.1) are located within some limited domain centered around the origin of the phase space, and therefore the right-hand side of this condition (equation 3.8) for every attractor of the system is less than some finite value.

We consider a positive function that has one minimum at the origin of phase space

$$U = \sum_{k=1}^{2} \left\{ \frac{x_k^2}{2} + \frac{y_k^2}{2b^2} + \frac{z_k^2}{2rS} \right\}. \tag{A.1}$$

The time derivative of this for the system (equation 3.1) is

$$\begin{aligned} \frac{dU}{dt} = & \frac{Sc_x^2}{2} - \epsilon(x_1 - x_2)^2 \\ & + \sum_{k=1}^{2} \left\{ -\frac{1}{S}\left(z_k + \frac{c_x S}{2}\right)^2 - \frac{1}{(4b)^2}(4y_k - 1 + b^2 x - bx^2)^2 \right. \\ & \left. + F(x_k) \right\}. \end{aligned} \tag{A.2}$$

where

$$F(x) = -\frac{3}{4}x^4 - \frac{(1 + b^2 x)x^2}{2b} + \frac{(1 + b^2 x)^2}{16b^2} + ax^3 + lx. \tag{A.3}$$

One can see from equation A.3 that $F(x)$ is positive when $|x| < E$ and has negative values for $|x| \geq E$. It follows from equation A.2 that in regions far enough from the origin, the time derivative dU/dt is negative, and therefore all trajectories beginning in this region are attracted by a domain centered at the origin of phase space.

Acknowledgments

The work of H. D. I. Abarbanel, N. F. Rulkov, and M. I. Rabinovich was supported in part by the U.S. Department of Energy, Office of Basic Energy Sciences, Division of Engineering and Geosciences, under contract DE-FG03-90ER14138 and DE-FG03-96ER14592, and in part by the Office of Naval Research (Contract N00014-91-C-0125). R. Huerta is supported by a (M. E. C.) Spanish Government Fellowship. A. I. Selverston and P. F. Rowat are supported by National Science Foundation Grant IBN-9122712.

References

Abarbanel, H. D. I. 1995. *Analysis of Observed Chaotic Data*. Springer-Verlag, New York.

Abarbanel, H. D. I., Brown, R., Sidorowich, J. J., and Tsimring, L. 1993. The analysis of observed chaotic data in physical systems. *Reviews of Modern Physics* **65**, 1331–1392.

Abarbanel, H. D. I., and Kennel, M. B. 1993. Local false nearest neighbors and dynamical dimensions from observed chaotic data. *Phys. Rev. E* **47**, 3057–3068.

Adams, W. B., and Benson, J. 1985. The generation and modulation of endogenous rhythmicity in the *Aplysia* bursting pacemaker neuron R15. *Prog. Biophys. Mol. Biol.* **46**, 1–49.

Afraimovich, V. S., Verichev, N. N., and Rabinovich, M. I. 1986. General synchronization. *Izv. VUZ. Radiophiz.* **29**, 795–803.

Aihara, K., and Matsumoto, G. 1986. Chaotic oscillations and bifurcations in squid giant axons. In *Chaos*, pp. 257–269. Manchester University Press, Manchester.

Fraser, A. M., and Swinney, H. L. 1986. Independent coordinates for strange attractors. *Phys. Rev.* **33A**, 1134.

Fujisaka, H., and Yamada, T. 1983. Stability theory of synchronized motion in coupled-oscillator systems. *Prog. Theor. Phys.* **69**, 32–47.

Gallager, R. G. 1968. *Information Theory and Reliable Communication*. John Wiley, New York.

Guckenheimer, J., and Holmes, P. 1983. *Nonlinear Oscillations, Dynamical Systems, and Bifurcations of Vector Fields*. Springer Verlag, New York.

Han, S. K., Kurrer, C., and Kuramoto, Y. 1995. Dephasing and bursting in coupled neural oscillators. *Phys. Rev. Lett.* **75**, 3190.

Hayashi, H., and Ishizuka, S. 1992. Chaotic nature of bursting discharges in the *Onchidium* pacemaker neuron. *J. Theor. Biol.* **156**, 269–291.

Hindmarsh, J. L., and Rose, R. M. 1984. A model of neuronal bursting using three coupled first order differential equations. *Proc. R. Soc. Lond. B* **221**, 87–102.

Heagy, J. F., Carroll, T. L., and Pecora, L. M. 1994. Experimental and numerical evidence for riddled basins in coupled chaotic systems. *Phys. Rev. Lett.* **73**, 3528–3531.

Hodgkin, A. L., and Huxley, A. F. 1952. A quantitative description of membrane current and its application to conduction and excitation in nerve. *J. Physiol. (London)* **107**, 500–544.

Kennel, M. B., Brown, R., and Abarbanel, H. D. I. 1992. Determining minimum embedding dimension using a geometrical construction. *Phys. Rev. A* **45**, 3403–3411.

Mpitsos, George J., Burton, R. M., Creech, H. C., and Soinla, S. S. 1988. Evidence for chaos in spike trains of neurons that generate rhythmic motor patterns. *Brain Res. Bull.* **21**, 529–538.

Oseledec, V. I. 1968. A multiplicative ergodic theorem. Lyapunov characteristic numbers for dynamical systems. *Trudy Mosk. Mat. Obsc.* **19**, 197.

Rabinovich, M. I., Huerta, R., Abarbanel, H. D. I., and Selverston, A. I. 1996. A minimal model for chaotic bursting of the LP neuron in lobster. Submitted to *Proc. Natl. Acad. Sci.*

Rinzel, J., and Ermentrout, G. B. 1989. Analysis of neural excitability and oscillations. In *Methods in Neuronal Modeling*, C. Koch and I. Segev, eds., pp. 135–160. MIT Press, Cambridge, MA.

Rose, R. M., and Hindmarsh, J. L. 1985. A model of thalmic neuron. *Proc. Roy. Soc. Lond. B* **225**, 161–193.

Rulkov, N. F., Volkovskii, A. R., Rodriguez-Lozano, A., Del Rio, E., and Velarde, M. G. 1992. Mutual synchronization of chaotic self-oscillators with dissipative coupling. *Int. J. Bif. Chaos* **2**, 669–676.

Selverston, A. I. 1996. Experiments on neurons within the STG Central Pattern Generator. Unpublished.

Sherman, A. 1994. Anti-phase asymmetric aperiodic oscillations in excitable cells—I. Coupled bursters. *Bull. Math. Biol.* **56**, 811–834.

Sherman, A., and Rinzel, J. 1992. Rhythmogenic effects of weak electrotonic coupling in neuronal models. *Proc. Natl. Sci. U.S.A.* **89**, 2471.

Skinner, F. K., Kopell, N., and Marder, E. 1994. Mechanisms for oscillation and frequency control in reciprocally inhibitory model neural networks. *J. Comp. Neuro.* **1**, 69.

Takens, F. 1981. In *Dynamical Systems and Turbulence, Warwick 1980. Lecture Notes in Mathematics* **898**, D. Rand and L. S. Young, eds., p. 366. Springer, Berlin.

Vreeswijk C., Abbott, L. F. and Ermentrout G. B. 1994. When inhibition not excitation synchronizes neural firing. *J. Compu. Neuro.* **1**, 313–321.

Received December 6, 1995; accepted March 26, 1996.